NUMERICAL SIMULATION OF THE INTERACTIONS OF HIGHLY ENTANGLED POLYMERS WITH COHERENT STRUCTURE IN A TURBULENT CHANNEL FLOW

Yoshimichi Hagiwara, Hidetoshi Hana, Mitsuru Tanaka and Susumu Murai
Dept. of Mechanical and System Engineering
Kyoto Institute of Technology
Matsugasaki, Sakyo-ku, Kyoto 606-8585, Japan

ABSTRACT

Direct numerical simulations have been conducted with many cluster models of beads and connecting springs in the buffer region of a turbulent channel flow in order to investigate how the low-speed streaks, the high-speed streaks and the flow related to the streaks are affected by the cluster models. The cluster model represents highly entangled polymers. The computational results show that the minor streaks and the small-scale eruptive flows associated with the low-speed streaks, whose length scale and time scale are comparable to those of the cluster model, are attenuated preferentially by the clusters.

INTRODUCTION

Near-wall coherent structures in turbulent channel flows of dilute polymer solutions have been focused on in order to understand the mechanism of drag reduction by polymers. Oldaker and Tiederman (1977) measured an increase in the spacing of low-speed streaks caused by Polyethylene Oxide (PEO) or Polyacrylamide (PAM). Tiederman *et al.* (1985) reported a decrease in the bursting rate and an increase in the streak spacing for a water channel flow with an injection of dilute PAM solutions from a slot into a buffer region.

The effect of the polymers on the coherent structure has been examined numerically recently in more detail. Direct numerical simulation (DNS) was used for the solvent flow, and the finitely-extendable-nonlinear-elastic (FENE) models were adopted as representative of polymer chains. This model consists of two spherical beads and a connecting spring with a nonlinear spring constant. Massah and Hanratty (1997) predicted an additional dissipation of energy by use of several FENE models in their DNS. Kajishima and Miyake (1998) reproduced the reduction of Reynolds shear stress and an increase in streak spacing using many beads-spring-dashpot models in their DNS.

We developed a cluster model of beads and springs as representative of highly entangled polymers because it seemed unlikely that it was possible that the entangled polymers were simulated with the FENE model (Hagiwara *et al.* 1997). Our model was based on irregular network structures in bundles of polymers, which were observed in the freeze-dried samples from the flows of dilute PEO solutions by James and Saringer (1980) and Miyamoto (1994). We carried out DNS on turbulent channel flow with the cluster models in the buffer region and showed the quasi-streamwise vortices were influenced by the models (Hagiwara *et al.* 1998). However, interactions between the streaks and the clusters have not yet been examined in detail.

In the present study, the effects of the cluster models in the buffer region on the Reynolds shear stress product are examined. Also, the length and time scales of the cluster and the streaks are investigated.

CLUSTER MODEL OF BEADS AND SPRINGS

Assumptions

Figure 1(a) shows the sketch from a photograph in Miyamoto's work. Strands which consist of a bundle of polymer chains and nodes where the strands are entangled are recognised in the irregular network structure in the photograph. We assumed that the nodes were replaced by spherical beads whose density is the same as that of the solvent flow. This is reasonable because the nodes take a long time for their dissolution and the nodes can be considered to be impermeable for a certain period of the dissolution. It was also assumed that the beads are of identical size, for simplicity.

Next, we assumed that the strands were replaced by nonlinear springs with no volume. The restitution force of springs was similar to that of an FENE model, and the spring constant was identical. If the distance between any two beads

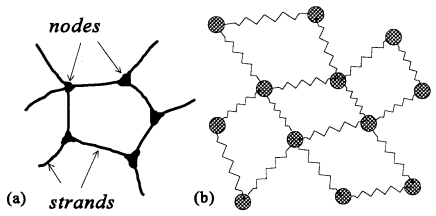

Figure 1. Observed polymers and cluster model

was longer than a certain length, l_c, these beads were assumed not to be connected directly by a spring. New entanglement of polymers or the formation of the network structure can be achieved by adding springs between the beads, while the breakup of the structure can be achieved by subtracting the springs. Figure 1(b) illustrates part of the cluster.

Finally, the connection between any two beads of two different cluster models was not considered for simplicity. This is reasonable when the polymer concentration is low and not completely uniform.

Motion of Beads

The drag force, $\boldsymbol{F}_D$, calculated by the Stokes law of resistance and the restitution force of the spring, $\boldsymbol{F}_S$, were considered to act on the beads. The equation of motion for the m-th bead is as follows:

$$\rho\frac{4\pi r^3}{3}\frac{\partial \boldsymbol{U}^m}{\partial t} = -\boldsymbol{F}_D^{\,m} + \boldsymbol{F}_S^{\,m} = -6\pi\mu r(\boldsymbol{U}^m - \boldsymbol{U}) + \sum_{n=1}^{N} \frac{k}{1-(l_{mn}-l_{mn0})^2/l_{mn0}^2}\frac{l_{mn0}-l_{mn}}{l_{mn}}(\boldsymbol{X}^m - \boldsymbol{X}^n) \tag{1}$$

where ρ is the bead density, r is the bead radius, $\boldsymbol{U}^m$ and $\boldsymbol{U}$ are the velocities of the bead and the solvent flow at the bead's location respectively, μ is the solvent viscosity, N is the total number of springs connected to the m-th bead, l_{mn} and l_{mn0} are the distance between the bead and the n-th bead and its unloaded value respectively, $\boldsymbol{X}^m$ and $\boldsymbol{X}^n$ are the positions of the m-th and n-th beads respectively, and k is the spring constant.

$\boldsymbol{U}^m$ was evaluated by the time integration of a discrete form of Eq. (1). The second-order Adams-Moulton method was used for the time integration. Note that the Reynolds number based on the bead diameter and the velocity difference between the bead and the ambient fluid was lower than 1.5, and hence the Stokes law was satisfied. The location of the bead was calculated by the second-order Adams-Moulton method (Pan and Banerjee, 1996).

Length Scales and Spring Constant

Table 1 compares the dimensions for the highly entangled polymers estimated from the results by Miyamato and the present authors (See Appendix B) with those for the cluster model in the present study. These values are in the nondimensional forms by using the friction velocity, u^*, of the present DNS, the kinematic viscosity, ν, and the channel height in our experiment. The values with brackets in the table indicate the initial values. The underlined value in the table denotes the experimental result by the present authors. The cluster volume in the table is calculated from the initial region of either $29.4\,\nu/u^* \times 7.4\,\nu/u^* \times 14.7\,\nu/u^*$ (rectangular prisms) or $14.7\,\nu/u^* \times 14.7\,\nu/u^* \times 14.7\,\nu/u^*$ (cube) for each cluster. We estimated the apparent spring constant from Miyamoto's discussion in which he calculated the stress, and the ratio of the length in the shear direction for a mesh in the network structure and that perpendicular to the direction. It is found from this table that all the values for the cluster model are realistic and reasonable.

TABLE 1. PARAMETERS OF THE CLUSTER MODEL

	Miyamoto	cluster model
shear rate	0.28	0.2~1.0(buffer region)
concentration [ppm]	500	600(buffer region)
node (bead) diameter	0.24~0.56	1.0
strand thickness	0.075~0.15	0
strand length	1.05~3.0	[3.6]
critical length	-	4.6
cluster volume	$\underline{1.5\sim12\times10^3}$	$[3.2\times10^3]$
node number density	0.032	[0.020]
spring constant	0.27	0.2

The unloaded spring length, l_{mn0} , was assumed to be equal to the spring length at the initial state.

Relaxation Time

We examined the relaxation time for the FENE model (Massah *et al.* 1993), λ, and that for one cluster, τ. These relaxation times are defined by the following equation.

$$\lambda = \frac{6\pi\mu r}{k} \qquad \tau = \frac{(1/6)\rho\pi D^3}{3\pi\mu D} = \frac{\rho D^2}{18\mu} \tag{2}$$

where D is the equivalent diameter of the cluster. λ can be considered as the relaxation time for a pair of beads connecting by a spring in the cluster. τ can be regarded as the relaxation time for the cluster behaving as a solid body due to the tight connection of the beads. λ was equal to $0.31\,\nu/u^{*2}$, and τ was $1.3\,\nu/u^{*2}$. The actual characteristic time for the cluster is expected to be in between these relaxation times for two extreme cases.

DNS FOR SOLVENT FLOW

Momentum Equation

The interaction between the bead of the cluster models and the flow was dealt with as a two-way coupling. The reaction force to the drag force in Eq.(1) was considered to act on the solvent flow as an external point force. The momentum equation of the flow is given as follows:

$$\frac{D\boldsymbol{U}}{Dt} = -\nabla\frac{P}{\rho} + \frac{\mu}{\rho}\nabla^2\boldsymbol{U} + \frac{1}{\rho V}\sum_{m=1}\boldsymbol{F}_D^{\,m} \tag{3}$$

where P is the pressure and V is a cell volume for the reaction force. All the fluid properties were assumed to be equal to that of a Newtonian fluid and constant.

Computational Domain

The computational domain was assumed to be a box of $2\pi h \times 2h \times \pi h$ for a flow between two walls at the distance of $2h$. The origin of the coordinates was at the corner of the lower wall. The X_1, X_2 and X_3 axes were positioned in the streamwise, wall-normal and spanwise directions, respectively. The domain was divided into a total of $64 \times 96 \times 64$ cells. The cell dimension is identical either in the X_1 or the X_3 direction. It increases from the walls to the axis based on a hyperbolic tangent. The velocity components were assigned at the centre of the cell surfaces (grid points for velocities), and the pressure and the external force were assigned at the centre of the cell (grid points for forces). The Reynolds number based on h and u^* was 150. The Reynolds number defined by the mean centerline velocity and the wall distance was 5306. In Table 2, the domain size, the number of grid points, the grid spacing, and the Reynolds number are compared with; those adopted in DNSs for channel flows with the polymer models (Massah and Hanratty; Kajishima and Miyake) and those without the models (Kawamura, 1995; Kuroda *et al.*, 1995).

Computational Schemes

The second-order central difference scheme based on the interpolation method (Kawamura, 1995; Kajishima, 1994; See Appendix A) and that without the method were applied to the finite differencing of the convection terms and the viscous terms of the momentum equations, respectively. The second-order Adams-Bashforth method was used for the explicit time integration of the convection terms, the viscous terms and the external-force terms. The fractional-step method was adopted for the implicit time integration of the pressure terms. These schemes were validated by comparing the turbulence quantities with those calculated by other DNS's by one of the present authors (Hana, 1999).

In the discretised form of Eq. (3), the reaction force to F_D for each bead was distributed to eight neighbouring grid points for forces by a spatial interpolation method. Similarly, the fluid velocity near a bead in the right-hand side of Eq. (1) was calculated from the values at eight neighbouring grid points for velocities by the spatial interpolation method.

Initial and Boundary Conditions

The result of a preliminary computation without the cluster models was adopted as the initial velocity field of the main computation after a statistically developed state was confirmed. The universal velocity distribution superimposed on sinusoidal velocity fluctuation in the three directions was taken as the initial velocity field for the preliminary computation. This velocity field satisfied the local and overall mass conservation.

200 cluster models were distributed nearly uniformly in the buffer region ($10 < X_2^+ < 25$) of the database at the initial state. This distribution is based on the experiments carried out by Tiederman *et al.* and the present authors shown in Appendix B. The initial location of the beads was nearly uniform in the initial cluster region mentioned above.

TABLE 2. DOMAIN SIZE AND GRID RESOLUTION

case	L_1/h	L_3/h	N_1	N_2	N_3	ΔX_1^+	ΔX_2^+	ΔX_3^+	Re^*
Present	2π	π	64	97	64	14.7	0.85~5.4	7.36	150
Kajishima	7.7	3.8	64	64	64	18	0.93~9.0	9.0	150
Massah (without polymer model)	13	6.3	128	65	128	14.8	NA	7.42	150
Kawamura	6.4	3.2	128	66	128	9.0	0.8~11.8	4.5	180
Kuroda	5π	2π	128	96	128	18.4	0.08~4.9	7.4	150

The nonslip boundary condition was imposed for the walls. The periodical boundary condition was applied for velocity components and pressure in the X_1 and X_3 directions.

RESULTS AND DISCUSSION

Coherent Structure Near the Clusters

We defined the low-speed streaks as the regions where $u_1 < -3.0u^*$ (u_1 is the fluctuating component of the streamwise velocity), and the high-speed streaks as the region where $u_1 > 3.0u^*$. The high-speed streaks are regarded as the core of sweeps. The area in which the absolute values of the streamwise vorticity are larger than $0.2u^{*2}/\nu$ was regarded as that of the quasi-streamwise vortices based on the DNS study by Tsujimoto and Miyake (1998).

Figure 2 shows a snapshot of the clusters in black, the low-speed streaks in dark grey and the high-speed streaks in light grey in the bottom half of the computational domain. Most clusters in the first and second rows from the transverse boundary in the upper left of the domain are found to be inside or near the low-speed streaks. Several clusters in the third and sixth rows are inside the high-speed streak. A few clusters in the fourth, fifth and seventh rows are near the minor low-speed streaks or the minor high-speed streaks. Many clusters in the eighth, ninth and tenth rows are near or inside the large-scale low-speed streak. The lift up and diffusion associated with the ejection and the bursting are observed in this streak.

In Table 3, the spanwise length and the characteristic time of the cluster are compared with the spanwise length and the duration of the streaks in the present computation. The data with brackets in the table are based on the summary by Meng (1998). The lengths of the minor streaks and the eruption of the low-speed streaks mentioned below are found to be comparable to that of the cluster.

Reynolds Shear Stress Product

Attenuation and Enhancement of Product. Figure 3 demonstrates the contour map of the difference between the Reynolds shear stress product with clusters and that without clusters in the plane $X_2^+ = 15$ at the same instant as that of Fig. 2. Broken lines indicate negative values of the difference, thus decreases in the values of the product. Solid lines indicate increases in the values of the product.

It is found by comparing Fig. 3 with Fig. 2 that the clusters near or inside the large-scale streaks enhance and attenuate the Reynolds shear stress product noticeably. The difference in the shear stress product reached more than $\pm 0.04u^{*2}$ in some narrow regions. This tendency was also observed in the case

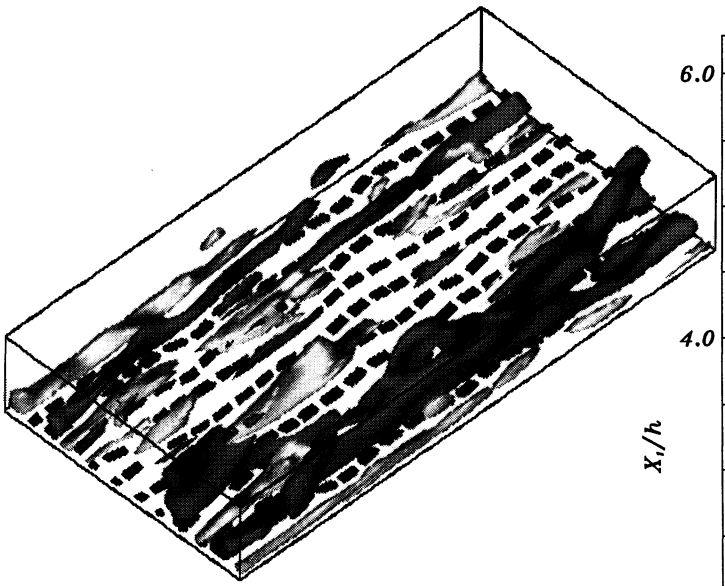

Figure 2. Snapshot of clusters and streaks (t^+=6.0)
(rectangular prism clusters)

TABLE 3. COMPARISON OF SCALES

	spanwise length	duration
cluster model	14.7	0.34 < t < 1.3
minor streaks	≅ 15	-
high-speed streaks	≅ 60 [< 100]	- [≅ 20]
low-speed streaks	≅ 40~70 [100]	- [≅ 480]
ejection	≅ 20 [10 ~ 30]	- [≅ 20]
eruption	≅ 15	< 4
streamwise vortices	≅ 40	-

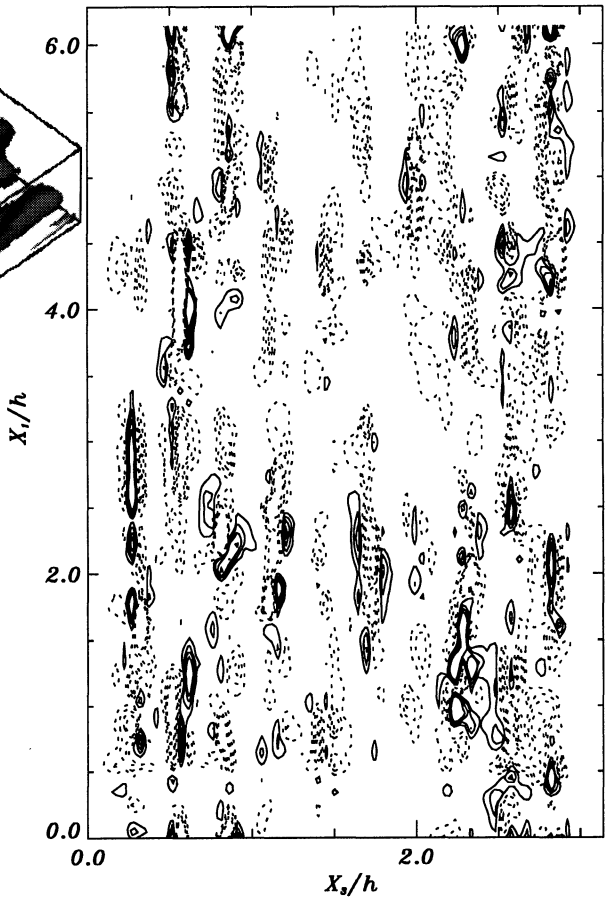

Figure 3. Contour map of the difference between the Reynolds shear stress product with clusters and that without clusters (contour interval = $0.01u^{*2}$)

where similar cluster models ware inside or near the streamwise vortices (Hagiwara *et al.*, 1997). Note that the interaction between the cluster and the streamwise vortices are not seen explicitly in the contour map because the cores of the vortices are located above this plane.

On the other hand, the clusters near the minor streaks are found not to enhance but to attenuate the shear stress product. The shear stress product decreased more than $-0.04u^{*2}$ and the outward fluctuating velocity $+u_2$ attenuated more than 5 percent. These results suggest that the interaction between the clusters and the minor streaks is different from that between the clusters and the large-scale streaks.

Streamwise Dimension of Contour. We compared the streamwise dimension, L_1, for the region in which the Reynolds shear stress product is affected with the distance, L_T, for the cluster to be transported for the period through which the cluster gives the reaction of the drag force, F_D', on the grid point. L_T was about $0.4h$ in this case. L_1 associated with the cluster irrelevant to the streaks is shorter than L_T. On the other hand, L_1 associated with the cluster near or inside the streaks is found to be longer than L_T even in the case of minor streaks. This shows that the modification of the fluctuating velocity around the distant cluster exerts an influence on the product through the velocity field even after the direct effect of the cluster vanishes. This suggests that the transport mechanism of turbulence is modified by the clusters. The aforementioned effects of the cluster were also observed in the case where the initial region for each cluster was the cube.

Minor Streak-cluster Interaction

We focused on the minor low-speed streak located at $4h < X_1 < 5h$ and $X_3 = 1.5h$ in Fig. 2. This is partly because this streak has a high possibility to develop into the large-scale streak, judging from the spanwise spacing of the low-speed streaks, and partly because the attenuations of the Reynolds shear stress product and the outward fluctuating velocity are noticeable.

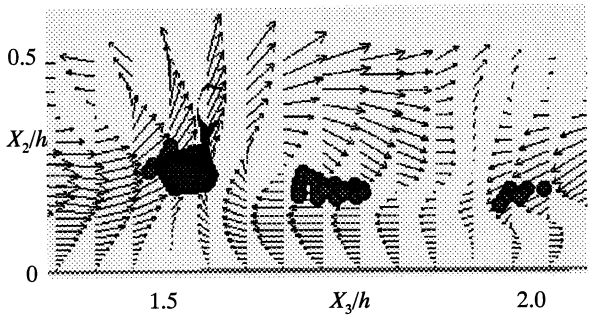

Figure 4. Velocity field in the (X_2, X_3)-plane at $X_1 = 4.9h$ with the cross sections of the minor streak and the beads

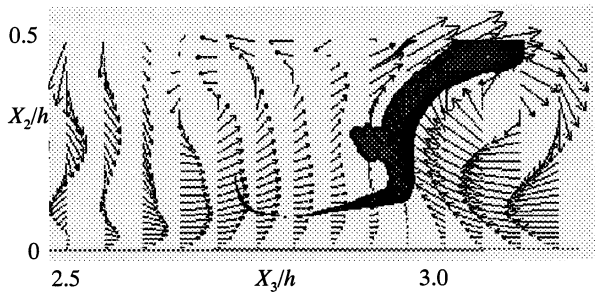

Figure 5. Velocity field in the (X_2, X_3)-plane at $X_1 = 0.54h$ with the cross sections of the large-scale streak and the beads

Figure 4 shows the velocity field in the (X_2, X_3)-plane at $X_1 = 4.9h$, including the cross sections of the minor streak in black and the beads of the cluster in solid circles. Note that the diameter of the beads is about three times larger the actual diameter. The flow from a left-hand side of the streak changed its direction from transverse to outward near the cluster and the streak. The cluster was deformed by this change in the flow direction, and therefore the drag force was generated on the beads. Then, $\boldsymbol{F}_D'$ acted as a resistance to the outward flow. Thus, the outward fluctuating velocity decreased, and the Reynolds shear stress product was attenuated. Since the spanwise length of the streak is comparable to the cluster dimension, this attenuation of the shear stress product occurred in the whole region of the streak. Therefore, the minor streak became inactive, and the evolution of the streak was prevented. This is expected to be one of the reasons of the decrease in the streaks observed by Tiederman *et al.*

Large-scale Streak-cluster Interaction

A noticeable attenuation of the Reynolds shear stress product is seen in the region around at $X_1 = 0.54h$, $X_3 = 2.7h$ in Fig. 3. This region corresponds to the tail of the large-scale low-speed streak. Figure 5 shows the velocity field in the (X_2, X_3)-plane at $X_1 = 0.54h$ including the cross sections of the large-scale streak in black and the beads of the cluster in solid circles. As shown in Table 3, this streak has a larger spanwise length and longer time scale compared with those of the cluster.

A strong outflow is observed to penetrate the thin streak. This flow was found to be characterised by the following events: u_2 increased with the distance from the wall in the buffer region, and a converged flow was induced by the outflow in the buffer region. The streamwise length of the outflow was not so long compared with the spanwise length of the flow (about $15\nu/u^*$). The duration was estimated to be shorter than $4\nu/u^{*2}$. From observations, this flow appears to be similar to the eruption of the low-speed streaks studied by Smith and Walker (1995). The eruption is considered to be followed by a bursting event.

Part of the outflow is found to approach the cluster. The strong drag force is generated on the beads by the nonuniform distribution of u_2 in the eruptive flow. Then, $\boldsymbol{F}_D'$ attenuates the outflows noticeably. $\boldsymbol{F}_D'$ also enhances the entrainment of ambient fluid in the dissipative part of the streak into the flow. The attenuation of the eruptive flow and the enhancement of the dissipative part cause equalisation of the outward velocity fluctuation. This equalisation may lead to an attenuation of the eruption and, therefore, an attenuation of the bursting. This can be a reason for the decrease in the bursting rate measured by Tiederman *et al.*

CONCLUSIONS

Direct numerical simulation was carried out for a turbulent channel flow with many cluster models of beads and springs representing highly entangled polymers in the buffer region. The main conclusions are as follows.

1. The minor streaks, which may develop into large-scale streaks, was attenuated by the cluster model whose spanwise length and duration are comparable to those of the minor streaks.
2. The cluster model attenuates the strong eruptive outward flows, whose spanwise length scale and relaxation time are comparable to those of the cluster, associated with the large-scale low-speed streaks.
3. These effects of the cluster model on the small scale near-wall coherent structure can be regarded as the cause of the observation made by Tiederman *et al.*

The authors acknowledge Dr. R. Nagaosa at National Institute of Resources and Environment, Japan for his comments on DNS.

REFERENCES

Hagiwara, Y., Takashina, Y., Tanaka, M. and Hana, H., 1997, "A Numerical Simulation on the Interaction between Tangled Polymers and Turbulent Structures," *Proc. 11th Turbulent Shear Flows*, Vol. 3, pp. 28-19 - 28-24.

Hagiwara, Y., Hana, H., Tanaka, M. and Maxey, M. R., 1998, "A Numerical Simulation on the Heat Transfer Attenuation due to Tangled Polymers in a Liquid Turbulent Channel Flow," *Proc. 11th Int. Heat Transfer Conf.*, Vol.4 pp253-258.

Hana, H., 1999, "Numerical Simulation on the Interaction between Entangled Polymer Chains and Turbulence Structure in a Flow of Dilute Polymer Aqueous Solution (in Japanese)," M. Sc. Thesis, Kyoto Inst. Technology.

Imamura, T., Murai, S., Hana, H., Hagiwara, Y. and Tanaka, M., 1999, "The Visualization of Polymer Clusters and Low-speed Streaks in a Duct Flow (in Japanese)," *Proc. 36th Heat*

Transfer Symp. of Japan, to appear.

James, D.F. and Saringer, J.H., 1980, "Extensional Flow of Dilute Polymer Solutions," *J. Fluid Mech.* Vol. 97, part 4, pp.655-671.

Kajishima, T., 1994, "Conservation Properties of Finite Difference Method for Convection (in Japanese)," *Trans. JSME*, Vol. 60B, pp. 2058-2063.

Kajishima, T. and Miyake, Y., 1998, "Drag Reduction by Polymer Additives in Turbulent Channel Flow Simulated by Discrete-Element Models (in Japanese)," *Trans. JSME*, Vol. 64B, pp. 3636-3643.

Kawamura, H., 1995, "Direct Numerical Simulation of Turbulence by Finite Difference Scheme," *The Recent Developments in Turbulence Research*, pp. 54-60 Int. Academic Publishers.

Kuroda, S., Kasagi, N. and Hirata, M., 1995, "Direct Numerical Simulation of Turbulent Plane Couette-Poiseuille Flows," *Turbulent Shear Flows 9*, (ed. by F. Durst *et al.*), pp. 241-257 Springer-Verlag.

Massah, H., Kontomaris, K., Schowalter, W. R. and Hanratty, T. J., 1993, "The Configurations of a FENE Bead-spring Chain in Transient Rheological Flows and in a Turbulent Flow," *Phys. Fluids*, Vol. A5, pp. 881-890.

Massah, H. and Hanratty, T. J., 1997, "Added Stresses Because of the Presence of FENE-P Bead-spring Chains in a Random Velocity Field," *J. Fluid Mech.*, Vol. 337, pp. 61-101.

Meng, J.C.S., 1998, "Wall Layer Microturbulence Phenomenological Model and a Semi-Markov Probability Predictive Model for Active Control of Turbulent Boundary Layers," *Self-sustaining Mechanisms of Wall Turbulence* (ed. R.L. Panton), pp.201-252, Comp. Mech. Pub.

Miyamoto, H., 1994, "Experiment for Visualization of Polymer Chains in High-polymer Aqueous Solutions under Shear Flow Regions (in Japanese)," *Trans. JSME*, Vol. 60B, pp. 2038-2043.

Oldaker, D. K. and Tiederman, W.G., 1977, "Spatial Structure of the Viscous Sublayer in Drag-reducing Channel Flows," *Phys. Fluids* Vol.20, S133-S144.

Pan, Y. and Banerjee, S., 1996, "Numerical Simulation of Particle Interactions with Wall Turbulence," *Phys. of Fluids*, Vol. 8, pp.2733-2755.

Smith, C.R. and Walker, J.D.A., 1995, "Turbulent Wall-layer Vortices," *Fluid Vortices* (ed. S.I. Green) pp.235-290, Kluwer Acad. Pub.

Tiederman, W. G., Luchik, T. S. and Bogard, D. G., 1985, "Wall-layer Structure and Drag Reduction," *J. Fluid Mech.* Vol.156, pp.419-437.

Tsujimoto, K. and Miyake, Y., 1998, "Identification of Quasi-streamwise Vortices in Near-wall Turbulence and Analysis of Self-sustenance Mechanism of Them (in Japanese)," *Trans. JSME,* Vol. 64B, pp.1989-1996.

APPENDIX A

In the second-order central difference scheme with the interpolation method, the gradient form of the convection term was evaluated not at the grid point but at half the grid-spacing in the direction of convection from the grid point. Then the interpolated value of two adjacent gradient forms in the direction of convection was assigned at the grid point between the two points where the forms were evaluated. This evaluation satisfies numerical consistency between the mass continuity and the momentum convection in case of uniform grid arrangement. Kawamura reported that the computational results of low-order turbulence quantities and the time change and the budget of turbulent kinetic energy using this scheme showed good agreement with the results obtained using the spectral method even in the case for nonuniform grid arrangement shown in Table 2.

The convection terms for the velocity of U_1 are expressed as follows;

$$
\begin{aligned}
&U_1\frac{\partial U_1}{\partial X_1}\Big|_{i+1/2,j,k} + U_2\frac{\partial U_1}{\partial X_2}\Big|_{i+1/2,j,k} + U_3\frac{\partial U_1}{\partial X_3}\Big|_{i+1/2,j,k} \\
&= \frac{1}{2}\Big[\Big(\frac{U_1|_{i+3/2,j,k}+U_1|_{i+1/2,j,k}}{2}\cdot\frac{U_1|_{i+3/2,j,k}-U_1|_{i+1/2,j,k}}{\Delta X_1} \\
&+ \frac{U_1|_{i+1/2,j,k}+U_1|_{i-1/2,j,k}}{2}\cdot\frac{U_1|_{i+1/2,j,k}-U_1|_{i-1/2,j,k}}{\Delta X_1}\Big) \\
&+ \Big(\frac{U_2|_{i+1,j+1/2,k}+U_2|_{i,j+1/2,k}}{2}\cdot\frac{U_1|_{i+1/2,j+1,k}-U_1|_{i+1/2,j,k}}{(\Delta X_2|_{j+1}+\Delta X_2|_j)/2} \\
&+ \frac{U_2|_{i+1,j-1/2,k}+U_2|_{i,j-1/2,k}}{2}\cdot\frac{U_1|_{i+1/2,j,k}-U_1|_{i+1/2,j-1,k}}{(\Delta X_2|_j+\Delta X_2|_{j-1})/2}\Big) \\
&+ \Big(\frac{U_3|_{i+1,j,k+1/2}+U_3|_{i,j,k+1/2}}{2}\cdot\frac{U_1|_{i+1/2,j,k+1}-U_1|_{i+1/2,j,k}}{\Delta X_3} \\
&+ \frac{U_3|_{i+1,j,k-1/2}+U_3|_{i,j,k-1/2}}{2}\cdot\frac{U_1|_{i+1/2,j,k}-U_1|_{i+1/2,j,k-1}}{\Delta X_3}\Big)\Big]
\end{aligned}
$$

where U_2 and U_3 are the velocity components in the X_2 and X_3 directions, respectively. The subscripts i, j and k denote the grid location in the X_1, X_2 and X_3 directions, respectively.

APPENDIX B

We conducted simultaneous visualisation of the low-speed streaks and the highly entangled PEO flowing in a duct of $2h$ = 20 mm in height at room temperature (Imamura *et al.* 1999). An aqueous dilute solution of Rhodamine B was injected into the fully-developed water flow in the duct from a transverse slot 1.0 mm in streamwise width at 45 degrees on the duct upper wall to enable visualisation of the low-speed streaks.

A dilute solution of PEO was introduced into the main flow from the other upstream slot. We adopted small pieces of an acrylic polymer emulsion colour as tagging material for highly-entangled PEO in the flow. These pieces were confirmed to stick to the polymer for a long time in the solution.

The images of the small pieces of the colour and the dye were captured by a progressive-scan video camera. The output signal of the video camera was directly recorded into a PC as digital images through a frame grabber. The Reynolds number based on the mean centerline velocity was 5.25×10^3.

It was observed in the captured images that the lifted away from the wall, the ejection and the breakup of the streaks occur if the group of colour pieces (that is highly-entangled polymers) is far from the wall and that the streak fluctuation was clearly attenuated when the group of colour pieces flows close to the streak. The dimension of the group was in the range of 0.94 ~1.9 mm.